Macromolecules

pubs.acs.org/Macromolecules Article

Relationship between Reaction Kinetics and Chain Dynamics of Vitrimers Based on Dioxaborolane Metathesis

Shilong Wu, Huanhuan Yang, Shaoyong Huang, and Quan Chen*

Cite This: *Macromolecules* 2020, 53, 1180−1190 Read Online

ACCESS | Metrics & More | Article Recommendations | Supporting Information

ABSTRACT: Processability of vitrimers strongly relies on the temperature dependence of viscosity. In this study, we analyzed temperature-dependent viscoelasticity of vitrimers based on the dioxaborolane metathesis reaction. A sol-to-gel transition process and a reverse gel-to-sol process are observed in the linear viscoelasticity with increasing content of the cross-linker. The latter gel-to-sol process is owing to a reverse reaction between a two-site interchain cross-linking point with an excess cross-linker, forming two noncross-linking sites. For samples above the gel point, the increasing temperature leads to a weaker acceleration of the decross-linking process than the Rouse-type relaxation, and accordingly, broadening of the plateau region. This trend is easily visualized in samples slightly above the gel point for which the stress relaxation arising from the Rouse-type relaxation and the decross-linking process are not well separated over time. This temperature-dependent behavior reflects a case that the lifetime of the dynamic covalent bond is significantly larger than the Rouse time of the network strands. As a result, the stress borne by a strand relaxes immediately upon decrosslinking, and thus, the low activation energy of the dioxaborolane metathesis reaction governs the strand relaxation.

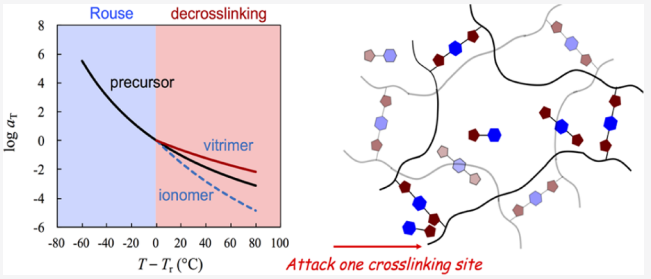

1. INTRODUCTION

Polymer networks can be classified into chemical and physical networks based on nature of the cross-linking bonds. A chemical network is formed from covalent cross-linking of bonding energy about two orders higher than the thermal energy at room temperature, endowing the chemical network with high stability. The chemical network is usually termed as the thermosetting material, that is, the material after thermal curing is "set" in shape, which deforms upon applying stress, and recovers its shape once the stress is unloaded. However, the material is not flowable.[1,2]

In comparison, a physical network is formed from physical interactions, such as hydrogen bonding,[3−10] ionic,[11−15] metal−ligand,[16−18] or host−guest[19−22] interactions and so on. Physical interactions usually have interaction energies either one order higher than or of the same order of the thermal energy.[1,2] Therefore, the lifetime of these interactions would approach the observable time scales at certain temperatures to enable reversibility of the materials. Materials based on these interactions could be reshaped upon heating to exhibit thermoplasticity. Although the physical network may become nonflowable after cooling down, it usually creeps upon applying stress and cannot resist polar solvents, particularly when the physical bonds are based on ionic groups that are electrostatic in nature.[1,2]

In order to develop materials that combine thermoplasticity and solvent resistance, one appealing pathway is to lower the activation energy so as to kinetically activate the chemical cross-linking and decrosslinking reactions. Several chemical reactions have demonstrated their suitability for this purpose, including Diels−Alder reaction,[23−26] disulfide−thiol exchange reaction,[27,28] transesterification reaction,[29−32] transamination reaction,[33−35] transcarbamoylation,[36,37] alkoxyamine exchange reaction,[38,39] siloxane equilibration,[40] dioxaborolane metathesis reaction,[41−43] and so on. Chemical networks based on these reactions are termed as covalent adaptable networks.[44]

Leibler and co-workers found unique rheology properties of a covalent adaptable epoxy network. This network exhibits a gradual Arrhenius-type decrease of viscosity with increasing temperature, which is analogous to that of the inorganic glasses. Leibler and co-workers thus termed this type of polymeric materials as "vitrimer".[45] The weak temperature dependence endows the epoxy network with great processability even if the temperature is not strictly controlled. Nevertheless, catalyst(s) should be introduced into the network to realize the reversibility, and thus stability and durability of the materials strongly rely on stability and amount of the catalyst(s).

More recently, Nicolaÿ, Leibler, and co-workers introduced a new class of catalyst-free vitrimer based on the dioxaborolane

Received: October 11, 2019
Revised: January 29, 2020
Published: February 13, 2020

https://dx.doi.org/10.1021/acs.macromol.9b02162
Macromolecules 2020, 53, 1180−1190

metathesis reaction.[46] The reaction can be realized under mild conditions without catalyst. Therefore, this vitrimer serves as a better system for studying the vitrimer dynamics. In fact, the dioxaborolane metathesis reaction has been extensively studied in recent years. Sumerlin and co-workers found that a degree of cross-linking of boronic ester-functionalized chain/block in solution could be tuned reversibly through changing a fraction of bifunctional cross-linker.[47,48] Guan and Ogden employed six-membered ring boroxine ($(BO)_3$) in constructing a thermoset with high malleability and recyclability.[49] Guo and co-workers introduced sacrificial metal−ligand coordination into the reversible boronic esters networks, and the materials thus-obtained exhibited remarkably enhanced mechanical performance without compromising the healing ability.[50] Nonetheless, the relationship between polymer dynamics and reaction kinetics of the functional groups remains to be elucidated.[51,52]

In this study, we investigate the relationship by designing a model vitrimer system based on the dioxaborolane metathesis reaction. We chose polymer matrix having a much lower T_g than those studied by Leibler and co-workers, that is, $T_g \approx 0$ °C for poly(hexyl methacrylate) in this study compared with $T_g \approx 100$ °C for polystyrene and poly(methyl methacrylate) (PMMA) studied by Leibler and co-workers.[46] The lower T_g enabled investigation of the dynamics of vitrimer samples over a wide T range without degradation.

The number of functional sites per chain was designed based on the Flory−Stockmayer mean-field theory. The theory considers interchain associations that are randomly placed on the precursor chains and predicts a gel point of $p_c = 1/(N-1)$, with N being a number of monomers per chain. This gel point corresponds to roughly one functional group per chain on average. Note that the random placement leads to a distribution of number of functional sites per chain; those chains containing no functional group are simply the solvent, those containing one functional group per chain are the dangling chains, and those containing two or more functional groups contribute to the formation of network. In this study, we attempted to fix a degree of polymerization N to be around 60, and change a number fraction p of the functional sites, and accordingly pN, an average number of functional sites per chain.

We found that when $pN = 0.7$, the network could not form owing to the insufficient functional sites per chain. When $pN = 1.9$ and 3.1, the interchain cross-linking reaction led to a sol-to-gel transition process. Surprisingly, we found that when the cross-linker is in excess, it reacted reversely with the cross-linking sites, leading to an additional gel-to-sol transition. Analysis of the linear viscoelasticity along with the sol-to-gel and gel-to-sol transitions enabled us to quantify dependence of a cross-linking number density on the content of cross-linker and accordingly the reaction constants of the dioxaborolane metathesis reaction. Particularly, we analyzed temperature-dependent linear viscoelasticity of a vitrimer sample slightly above the gel point and found that the temperature dependence of the decrosslinking process is weaker than that of the Rouse-type relaxation. This result is explained as owing to the much slower decrosslinking reaction compared with the Rouse relaxation of the network strands. As a result, the strand relaxation is controlled by the low activation energy of the dioxaborolane metathesis reaction. Details are explained in this paper.

2. EXPERIMENTAL SECTION

2.1. Materials. We synthesized three poly(hexyl methacrylate-random-2,3-dioxaborolanepropyl methacrylate) precursor samples through the reversible addition−fragmentation chain transfer (RAFT) reaction, with 2-cyanoprop-2-yl-dithiobenzoate utilized as the RAFT agent. Gel permeation chromatography measurements were performed at ambient temperature on Wyatt Optilab equipped with low-angle light scattering (LALS) and reflective index (RI) monitors, with tetrahydrofuran (THF) utilized as an eluent. The flow rate was 1 mL/min and concentration of the solution was 2.0 mg/mL. M_w was determined from LALS with $dn/dc = 0.0829$, and M_w/M_n was determined from the RI signal. In this study, $M_n \approx 10$ kDa of the precursors was much larger than $M = 221$ Da of the RAFT agent. From M_n we determined the degree of polarization $N \approx 60$ (Table 1),

Table 1. Important Parameters of all Precursor Samples

samples pN-r	N	M_n (kDa)	M_w/M_n	ϕ_p^B (ppm)	T_g (°C)
0.7−0	60	10	1.15	670	−6
1.9−0	60	10	1.2	1800	−1
3.1−0	59	9.7	1.3	2700	9

which was the same as we designed. Boron elemental analysis was conducted to determine the boron content of the precursor ϕ_p^B and accordingly an average number pN of boron-containing monomer(s) per chain.[48] These boron-containing sites were cross-linked by a bifunctional cross-linker, that is, 2,2′-(1,4-phenylene)-bis[4-methyl-1,3,2-dioxaborolane]. Chemical structures of the precursor and cross-linker are shown in Figure 1a, and the important parameters of the three precursors are summarized in Table 1.

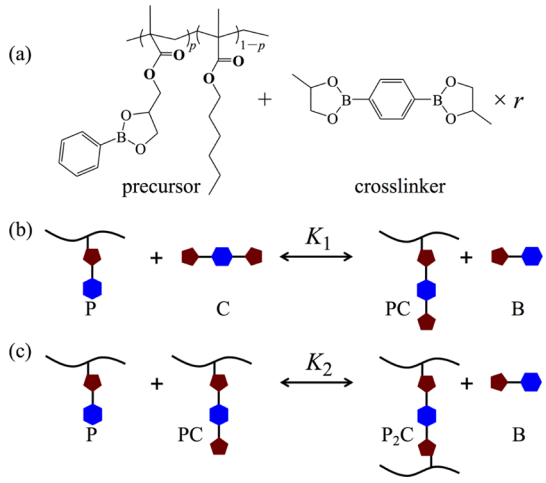

Figure 1. (a) Chemical structures of precursor and cross-linker, (b) first and (c) second step of the dioxaborolane metathesis reaction, with K_1 and K_2 as the reaction equilibrium constants, respectively. The products in the first and second reactions are PC and P_2C, respectively, and the byproduct is B.

On assumption of random copolymerization, a probability of a number of functional sites per chain, f, can be calculated from the binary distribution as

$$P(f;p,\ N) = \frac{N!}{(N-f)!f!}p^f(1-p)^{N-f} \quad (1)$$

In Figure 2, the predicted $P(f)$ is plotted against f for the three precursor samples in this study, with $pN = 0.7$, 1.9, and 3.1 as indicated in arrow. For $pN = 0.7$, the majority of the chains have only 0 and 1 functional sites. Therefore, this precursor is unlikely to form a network. In comparison, the majority of the chains have 2 or more sites per chain for $pN = 1.9$ and 3.1, which may be cross-linked into a

https://dx.doi.org/10.1021/acs.macromol.9b02162
Macromolecules 2020, 53, 1180−1190

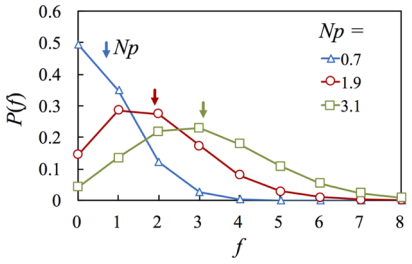

Figure 2. Binomial distribution function $P(f)$ of polymer chains having f functional sites. The average number of functional monomer(s) $pN = \Sigma f P(f)$ are indicated in arrow.

network when suitable amount of cross-linker is introduced. This expectation has been confirmed in our study. Namely, the network cannot be formed for the samples with $pN = 0.7$, whereas clear sol-to-gel transition can be observed for the samples with $pN = 1.9$ and 3.1. In this study, the analyses of reaction kinetics and rheological results will be focused on the samples with $pN = 1.9$, and the results of the samples with $pN = 0.7$ and 3.1 will be summarized in the Supporting Information.

To prepare the vitrimer samples, we mixed the precursor and cross-linker at various cross-linker/precursor molar ratios r. The vitrimers are thus coded as pN-r (with $r = 0$ indicates the precursor). Both components were dissolved in 10 mL anhydrous THF and stirred at 60 °C for 10 h to complete the reaction.

Figure 1b explains the two-step dioxaborolane metathesis reaction between the precursor and cross-linker. In the first step, one functional site of the bifunctional cross-linker, denoted as C, is exchanged with one cross-linkable site of the precursor chain, denoted as P, to form one one-site cross-linked product PC and one small molecular byproduct B (phenylboronic acid 1,2-propanediol ester). In the second step (Figure 1c), one additional P site is reacted with one PC site to form one two-site cross-linked product P_2C and one byproduct B. P and PC in the second-step reaction could belong to either the same chain or two different chains, forming intra- and inter-chain cross-links, respectively. After the reaction, the anhydrous THF was evaporated in oven at 80 °C for more than one week.

To check the evaporation of the cross-linker and the byproduct during the sample preparation, we conducted elementary analysis to determine a weight fraction of boron in the vitrimer products, ϕ^B_{pro}, to be compared with a weight fraction of boron in the reactants (i.e., mixtures of the precursor and cross-linker), ϕ^B_{rea}. The weight fraction of the reactants is calculated by

$$\phi^B_{rea} = w_p \phi^B_p + w_c \phi^B_c \quad (2)$$

Here, w_p and w_c are the weight fraction of the precursor and the cross-linker, respectively, ϕ^B_p and ϕ^B_c are the weight fraction of B within the precursor and cross-linker, respectively. ϕ^B_p was measured directly with elementary analysis, and ϕ^B_c was calculated from the molecular structure shown in Figure 1a.

To check an effect of the evaporation, ϕ^B_{pro} was detected and compared with ϕ^B_{rea} for the 1.9-r vitrimers in Table 2. We find $\phi^B_{pro}/\phi^B_{rea} \geq 95\%$ all samples except the two samples with the highest r, that is, $\phi^B_{pro}/\phi^B_{rea} = 88\%$ for 1.9−6.0 and 89% for 1.9−12. The higher evaporation of these two samples is attributable to their high flowability at 80 °C, as noted during the sample preparation. The main mechanism of this high flowability is the gel-to-sol transition that will be explained later. More details regarding the synthesis and characterization of the precursor, cross-linker, and vitrimers are explained in Schemes S1−S4 and Figures S1−S5 of the Supporting Information.

2.2. Rheological Measurements. All linear viscoelastic measurements were conducted on a stress-controlled rheometer (MCR-302, Anton Paar, Austria) using 8 mm parallel plates. Most of the samples were loaded at T higher than T_g + 60 °C where the samples could flow, while lower than 200 °C to avoid the sample degradation. The frequency sweep measurements were conducted in a range of 10−200 °C within the linear region as confirmed through the strain amplitude sweeps. All measurements were conducted in an environment of highly purified N_2 to avoid degradation. For each sample, the frequency sweep measurement was conducted in a frequency range of 10^2 to 10^{-1} rad/s (or 10^{-2} rad/s) from the lowest T (10 °C or higher) to the highest T (200 °C or lower) at 10 or 20 °C each step. After that, the temperature was cooled down to the lowest T where the reproducibility was checked. The data were reproducible in between the first and the last measurements, meaning that the evaporation of the small molecules played a negligible effect on the LVE data measured in this study.

3. REACTION KINETICS

The equilibration of the two-step reaction can be written as

$$K_1[P][C] = [PC][B] \quad (3)$$

$$K_2[P][PC] = [P_2C][B] \quad (4)$$

where K_1 and K_2 are the equilibrium constants of the first- and second-step reactions, respectively. Conservation of the functional sites of polymer gives

$$[P] + [PC] + 2[P_2C] = C \quad (5)$$

where C is the concentration of all functional polymer sites before the reaction. Similarly, conservation of the mono-dioxaborolane and bis-dioxaborolane sites gives, respectively

$$[P] + [B] = C \quad (6)$$

and

$$[C] + [PC] + [P_2C] = (r/pN) \times C \quad (7)$$

Table 2. Important Parameters of the 1.9-r Precursor and Vitrimer Samples

samples 1.9-r	r[a]	DP	M_n (kDa)	M_s (kDa)	M_w/M_n	ϕ^B_{rea}[b] (ppm)	ϕ^B_{pro}[c] (ppm)	$\phi^B_{rea}/\phi^B_{pro}$ (%)	T_g (°C)	T_{iso} (°C)[d]	ε[e]
1.9−0	0	60	10		1.2		1800	100	−1	60	−1
1.9−0.8	0.8					3150	3200	102	3	64	0
1.9−1.2	1.2			80		3850	3700	96	4	65	0.31
1.9−1.4	1.4			45		4200	4000	95	8	68	0.44
1.9−1.6	1.6			32		4550	4500	99	10	70	0.56
1.9−3.0	3.0			32		6800	6500	96	10	70	0.56
1.9−5.3	5.3			42		10,400	9900	95	4	67	0.46
1.9−6.0	6.0					11,400	10,000	88	2	60	0
1.9−12	12					19,200	17,000	89	−6	55	

[a]Molar ratio of cross-linker and precursor. [b]Weight fraction (in unit of ppm) of borate in the reactant. [c]Weight fraction (in unit of ppm) of borate in the product, which was determined from the elementary analysis with uncertainty within ±5%. [d]Iso-frictional reference temperature that is 61 °C higher than T_g. [e]Degree of gelation.

https://dx.doi.org/10.1021/acs.macromol.9b02162
Macromolecules 2020, 53, 1180−1190

In eq 6, the right side is the concentration C of mono-dioxaborolane sites of the polymer before the reaction, and the left side terms are those incorporated in the unreacted polymer sites and the byproduct after the reaction, that is, [P] and [B]. Equation 7 equals the concentration of bis-dioxaborolane sites $(r/pN) \times C$ of the cross-linker before the reaction, and those of the cross-linker, single- and dual-crosslinking points after the reaction, that is, [C], [PC], and [P_2C]. The factor r/pN specifies a molar ratio between the cross-linker and the functional sites of the precursor. This factor becomes $r/1.9 = 0.53r$ for the 1.9-r system. Equations 3−7 can be solved numerically to determine the normalized concentrations, [B]/C, [PC]/C, and [P_2C]/C, as functions of r, K_1, and K_2.

Figures 3 and 4 show the r dependences of [PC]/C and [P_2C]/C of the 1.9-r system for fixed $K_1 = 1$ and varied K_2 = 0.1, 1, and 10 and fixed $K_2 = 1$ and varied K_1 = 0.1, 1, and 10, respectively. In both figures, [P_2C]/C first increases and then decreases with increasing r, indicating that the degree of gelation first increases and then decreases with increasing r. In contrast, [PC]/C consistently increases with r and approaches 1 at $r \gg 1$, meaning that finally all the polymer sites are reacted into the non-crosslinked PC site when the cross-linkers are of great excess.

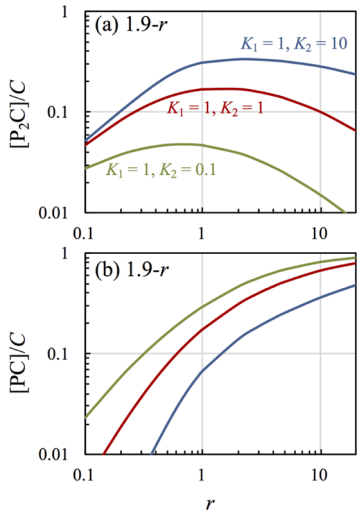

Figure 3. Model prediction of [P_2C]/C against r for the 1.9-r system, with given reaction constants $K_1 = 1$ and K_2 as indicated.

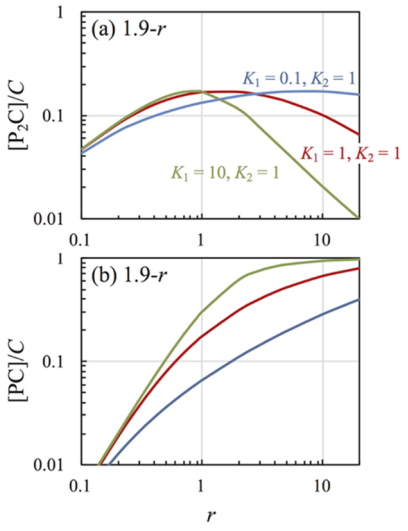

Figure 4. Model prediction of [P_2C]/C against r for the 1.9-r system, with given reaction constants $K_2 = 1$ and K_1 as indicated.

In Figure 3 where $K_1 = 1$ is fixed, the amplitude of the [P_2C]/C peak increases, and the peak position shifts to higher r value with an increase of K_2 that facilitates the formation of [P_2C]/C. Particularly, [P_2C]/C peaks near the equivalent point, that is, $r = 1$, when $K_2 = 1$, where the peak value of [P_2C]/C is ∼0.17, meaning that a fraction of polymer sites that join the two-site cross-linking point is ∼0.17/0.5 = 34% (0.5 is obtained on assumption of completion of the reaction of P sites into P_2C). This maximum fraction increases to 67% upon increasing K_2 to 10.

In Figure 4 where $K_2 = 1$ is fixed, the [P_2C]/C peak almost maintains the same amplitude, while its position shifts to higher r with decreasing K_1. This trend is due to the fact that the product of the first-step reaction, PC, is one of the reactants of the second step reaction. To achieve a similar level of [P_2C] in the second step reaction, more cross-linker (i.e., higher r) is needed when K_1 is smaller.

4. RESULTS

4.1. Glass Transition Temperature. Figure 5 shows the DSC traces of the 1.9-r system, with the value of r as indicated.

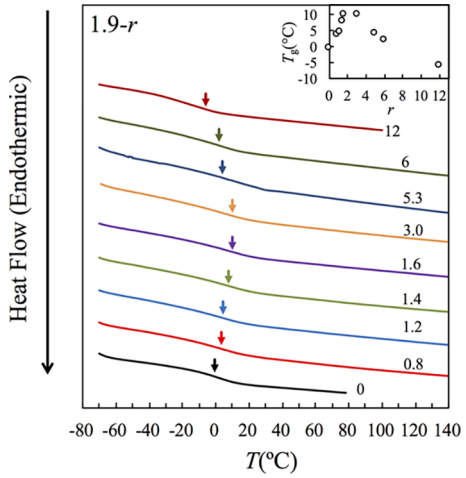

Figure 5. DSC traces of 1.9-r samples with the value of r as indicated. Inset plots T_g against r.

The glass transition temperature T_g as indicated in arrow first increases with r for $r \leq 1.6$ and then decreases with increasing r for $r \geq 3.0$. The former increase of T_g has been observed extensively in the chemical cross-linking system because the motion of polymer segments is restricted near the cross-linking sites. It is interesting that further increasing r from 3.0 to 12 leads to a decrease of T_g. The transition is more clearly seen in the inset where T_g is plotted directly against r, where we find that T_g first increases and then decreases with increasing r. The decrease of T_g with increasing r is associated with two mechanisms. The first mechanism is the decrosslinking; we note in Figures 3a and 4a that the effective cross-linking points, as indicated by [P_2C], first increases and then decreases with increasing r, the latter stage would lead to the decrosslinking to reduce T_g. Second, the abundant of cross-linker should plasticize the vitrimer sample, this effect can be seen through comparing T_g of the 1.9−0 ($r = 0$) and 1.9−12 samples ($r = 12$); T_g of 1.9−12 is even lower than that of the non-

https://dx.doi.org/10.1021/acs.macromol.9b02162
Macromolecules 2020, 53, 1180−1190

crosslinked precursor, indicating the strong plasticizing effect for this sample. Another feature of current system is that the glass transition process is broad. This feature should be partly related to introduction of the functional monomers that are less mobilized. As an evidence, we find in Table 1 that T_g increases with a content of the functional monomer.

4.2. Overview of Linear Viscoelasticity. The linear viscoelastic measurements were conducted for the 0.7-*r*, 1.9-*r*, and 3.1-*r* systems. All these systems show qualitatively a similar trend, that is, increasing *r* first leads to an increase and latter to a decrease of a degree of gelation. However, no rubbery plateau is observed for the 0.7-*r* system (Figure S6), probably because the average number of functional site(s) per chain is too small to allow the gelation (cf. Figure 2). In comparison, clear sol-to-gel transition followed by gel-to-sol transition is observed for the 1.9-*r* (Figures 6 and 7 below) and 3.1-*r* (Figures S7 and S8

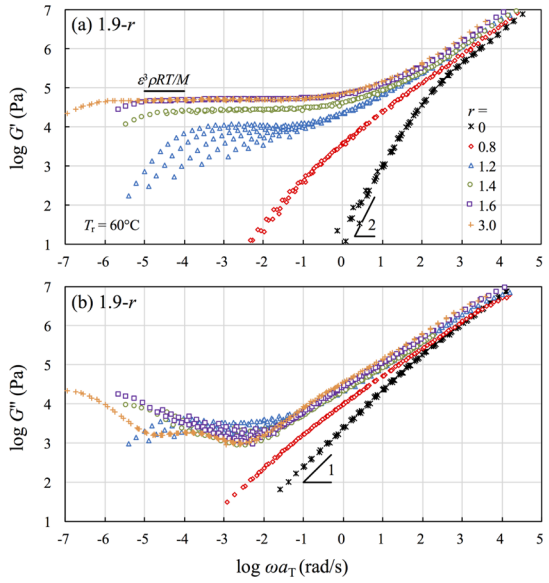

Figure 6. Comparison of pseudo-master curves of the storage and loss moduli, G' and G'', reduced at T_r = 60 °C for the precursor and 1.9-*r* vitrimer samples with *r* from 0 to 3.0.

of the Supporting Information) systems. Below, our analysis is focused on the 1.9-*r* system that is more thoroughly studied experimentally.

Figure 6 shows the (pseudo-) master curves of storage and loss moduli, G' and G'', plotted against reduced angular frequency, ωa_T, for the 1.9-*r* system, with *r* as indicated. The precursor chain (r = 0) shows a typical Rouse behavior characterized by a Rouse power-law region followed by the terminal tails, $G' \sim \omega^2$ and $G'' \sim \omega$, meaning that the precursor chains are nonentangled.

LVE of 1.9−0.8 is characterized by power law like behavior $G' \sim G'' \sim \omega^n$ at low ω before the terminal relaxation, reflecting the hierarchical relaxation of the sol chains. The power *n* is close to 0.67 predicted by the critical percolation model.[1,53] In comparison, the samples of $1.2 \le r \le 3.0$ show clear plateau, meaning that they are above the gel point. The amplitude of plateau increases with *r* for $r \le 1.6$, indicating that the network is densified with increasing *r*, which should be related to an increase of $[P_2C]$.

It is interesting that the amplitude of plateau is very similar for 1.9−1.6 and 1.9−3.0, meaning that $[P_2C]$ is similar for

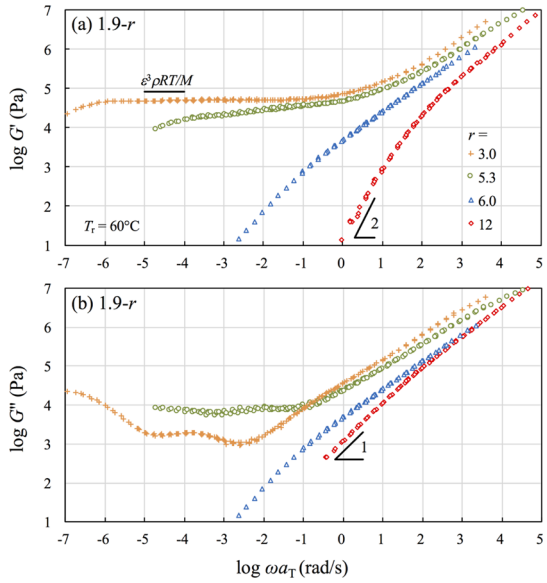

Figure 7. Comparison of pseudo-master curves of the storage and loss moduli, G' and G'', reduced at T_r = 60 °C for the 1.9-*r* vitrimer samples with *r* from 3.0 to 12.

these two samples. However, the decrosslinking process is lightly delayed for 1.9−3.0. This difference can be attributable to the difference of their non-crosslinked polymer sites, 1.9−1.6 should have more unreacted P sites but less PC sites than 1.9−3.0. Although both the P and PC sites do not contribute to the formation of network, the mobility could be lower for the latter, leading to the slower decrosslinking dynamics of 1.9−3.0.

Another interesting feature revealed in Figure 6 is that the time−temperature superposition (tTs) fails most significantly for the 1.9−1.2 sample that is just above the gel point, while this failure becomes less obvious when the degree of gelation is further increased. This trend will be discussed in the next section in more detail.

Figure 7 shows the (pseudo-) master curves of storage and loss moduli, G' and G'', for the 1.9-*r* vitrimer samples with further increasing *r* from 3.0 to 12. The excess cross-linker molecules lead to the gel-to-sol transition. This trend is predicted earlier in Figures 3a and 4a, where $[P_2C]$ decreases with increasing *r* at high *r*. This transition is owing to a reduction of $[P_2C]$ caused by reaction between P_2C and the excess *C*, yielding two non-crosslinked PC. The corresponding reaction function, $P_2C + C = 2PC$, can be obtained through subtracting the second step cross-linking function $PC + P = P_2C$ (Figure 1c) from $P + C = PC$ (Figure 1b), and the reaction equilibrium constant is thus ($K = K_1/K_2 = [PC]^2/([C][P_2C])$).

4.3. Time−Temperature Superposition. Figure 8 explains the method to construct the master curves of the representative samples. For all master curves, we chose T_r = 60 °C as the reference temperature, where the modulus attributed to the network starts to manifest. This feature can be seen as the nonsuperposing of the G' curves at 0.01 rad/s $\le \omega \le$ 100 rad/s, the ω range for the frequency sweep measurements at T_r, in Figures 6a and 7a.

After choosing T_r, we normalized the storage and loss moduli, G' and G'', measured at different T by an intensity factor $b_T = T_r/T$ and shifted $b_T G'$ and $b_T G''$ horizontally by a factor a_T to superpose the high ω Rouse part of modulus. If the

https://dx.doi.org/10.1021/acs.macromol.9b02162
Macromolecules 2020, 53, 1180−1190

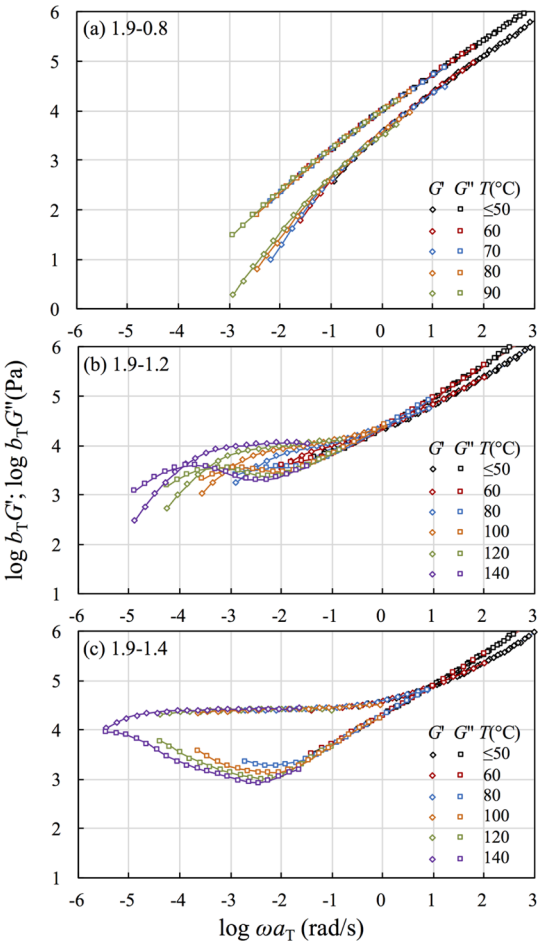

Figure 8. Test of tTs of the 1.9−0.8, 1.9−1.2, and 1.9−1.4 samples. The storage and loss moduli G' and G'' are normalized by a temperature factor $b_T = T_r/T$, and shifted by a factor a_T to superpose the high-ω Rouse part of modulus.

sample structure does not change with T, the modulus having entropic origin is proportional to ρT. Because a change of density with T is much smaller compared with a change of T itself, $b_T = T_r/T$ can be chosen approximately as an intensity factor. However, the structure may change with T, and thus to test the tTs of $b_T G'$ and $b_T G''$ in turn enables us to elucidate this change.

Figure 8a reveals slight failure of tTs for 1.9−0.8. Upon superposing the high ω G' and G'' ($\geq 10^3$ Pa), the power law region broadens, and the terminal relaxation shifts to lower ω with increasing T. This result suggests a trivial increase of degree of gelation with increasing T.

In contrast, to superpose the Rouse part of modulus of 1.9−1.2 (Figure 8b), that is, modulus at ω higher than the valley of G'', leads to significant failure of tTs at low ω. Because the plateau modulus of a network is proportional to $P_{gel}\rho RT/M_s$, where P_{gel} is the fraction of gel and M_s is the average molecular weight per network strand, and a change of ρT have been properly incorporated into our intensity factor b_T, the slight increase of amplitude of plateau with increasing T should reflect a trivial increase of the degree of cross-linking with increasing T, which is, in spirit, similar to that observed in Figure 8a. The plateau region broadens greatly with the increasing temperature, for example, increasing T from 100 to 140 °C leads to a broadening of the plateau region by a factor of ∼1 decade, which cannot be attributed to the trivial increase of degree of gelation.

The overall trend for LVE of 1.9−1.4 shown in Figure 8c and 1.9−1.6 shown in Figure S9 of the Supporting Information is qualitatively similar to that of the 1.9−1.2 sample. In Figure 8c, the broadening of the plateau region is less obvious than that in Figure 8b, owing to the higher degree of gelation and accordingly broader plateau that separates the Rouse and decrosslinking parts of modulus. In Figures 8b,c, the highest T is chosen to be 140 °C because the superposition is selectively given on the high-ω Rouse part, and this part becomes nondetectable at T higher than 140 °C.

It is informative to superpose G' and G'' obtained at high T where the decrosslinking process is dominant. In Figure 9, we

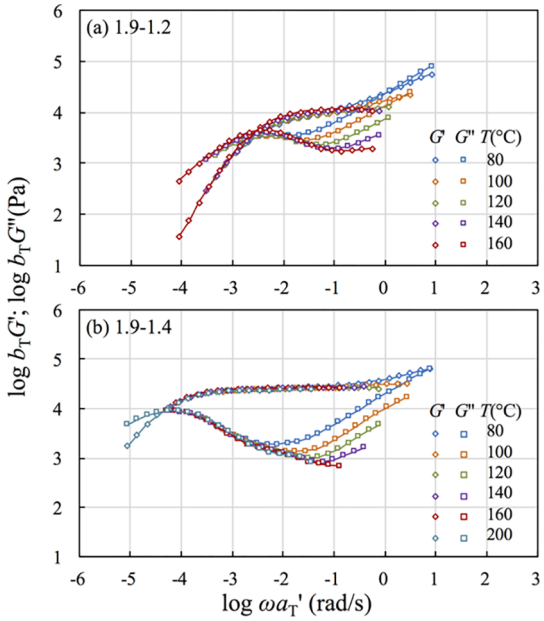

Figure 9. Test of tTs of the 1.9−1.2 and 1.9−1.4 samples. Normalized storage and loss moduli, $b_T G'$ and $b_T G''$, obtained at $T > 80$ °C are shifted by a factor a_T' to superpose the low-ω part of moduli to that at $T = 80$ °C, at which a_T' (in Figure 9) equals to a_T (in Figure 8).

choose $T = 80$ °C after the first-round shift (in Figures 8b,c) as the new reference and superpose the low-ω decrosslinking part of $b_T G'$ and $b_T G''$ of 1.9−1.2 (Figure 9a) and 1.9−1.4 (Figure 9b) at $T > 80$ °C through horizontal shift by a new factor, a_T'. The G' and G'' data can be reasonably superposed at low ω but not at high-ω, reflecting the broadening of the plateau region with increasing T.

4.4. Shift Factors and Activation Energy. The shift factors a_T for the master curves of the 1.9-r system shown earlier in Figure 6 (with $r \leq 3$) are plotted against $T - T_r$ in Figure 10a in unfilled symbols connected with curves, where a_T is obtained from superposing the high-ω Rouse part of modulus. The temperature dependence of a_T strengthens slightly with increasing r up to 3, owing mainly to increase of T_g therein (cf. Figure 5). To confirm on this point, we chose a new iso-frictional temperature $T_{iso} = T_g + 61$ °C ($T_{iso} = T_r$ for the precursor) and reevaluated the shift factor. A good agreement is found for the re-evaluated shift factor a_{iso} plotted against $T - T_{iso}$ in Figure 10b, lending support to the argument that the deviation of a_T seen in Figure 10a is owing

https://dx.doi.org/10.1021/acs.macromol.9b02162
Macromolecules 2020, 53, 1180−1190

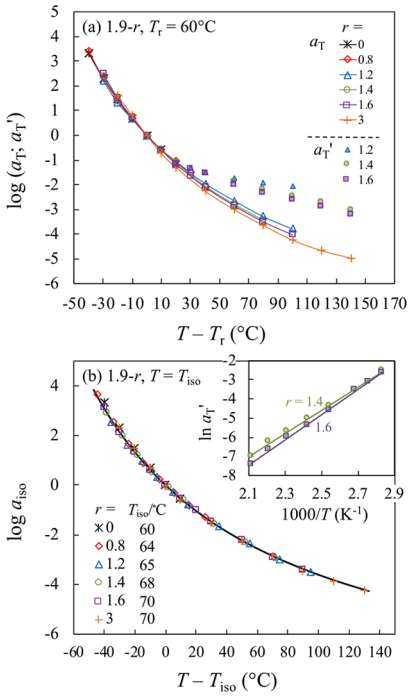

Figure 10. (a) LVE shift factor a_T in Figures 6 and 8, as represented by unfilled symbols connected in curve, and a_T' in Figures 9 and S9b, as represented by filled symbols, plotted against $T - T_r$ for the 1.9-r system, with r (≤3) values as indicated. (b) a_T in the top panel is reevaluated with respected to the new reference temperature $T_{iso} = T_g + 61$ °C ($T_{iso} = T_r$ for $r = 0$). The curve represents a prediction of WLF eq 8. Inset shows plots of ln a_T' against 1000/T for the 1.9−1.4 and 1.9−1.6 samples.

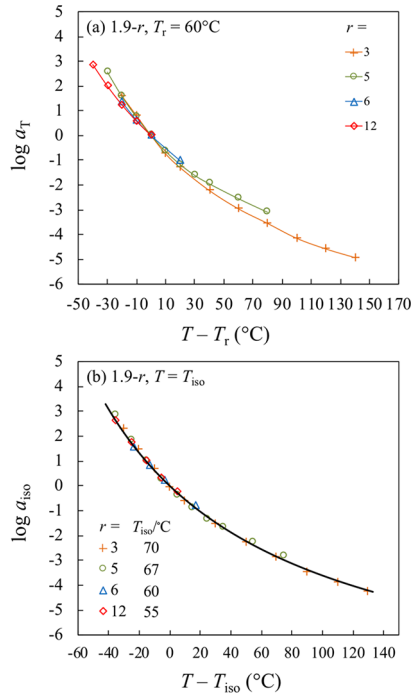

Figure 11. (a) LVE shift factor a_T in Figure 7, with r (≥3) values as indicated. (b) a_T in the top panel is reevaluated with respected to the new reference temperature $T_{iso} = T_g + 61$ °C ($T_{iso} = T_r$ for $r = 0$). The curve represents a prediction based on WLF eq 8.

to the difference of T_g. The plots in Figure 10b are fit well to the Williams−Landel−Ferry (WLF) equation

$$\log a_T = -9.5(T - T_r)/(163 + T - T_r) \quad (8)$$

In Figure 10a, the filled symbols represent shift factor a_T' obtained from superposing the low-ω decrosslinking part of modulus (in Figures 9 and S9b), whose temperature dependence is much weaker than that of a_T. The temperature dependence of a_T' is Arrhenius-type, which contrasts with the WLF-type temperature dependence of a_T. Linear fits to plots of ln a_T' against 1000/T (inset of Figure 10b) give the activation energy of E_a = 50 kJ/mol for 1.9−1.4 and 55 kJ/mol for 1.9−1.6. (We did not use a_T' data of 1.9−1.2 because it is slightly above the gel point where the relaxation time is sensitive to a degree of gelation that changes slightly with T.) These values are slightly larger than but still reasonably close to $E_a = 43 \pm 4$ kJ/mol determined by Leibler and co-workers through analyzing the relaxation modulus $G(t)$ of vitrimer samples based on the same functional sites but different polymer backbone (PMMA by Leibler et al.[46] and PHMA here).

Figure 11a compares the shift factor plotted against $T - T_r$ for the 1.9-r vitrimer samples having $r \geq 3$. The temperature dependence weakens as increasing r, reflecting a decrease of T_g therein. By choosing an iso-frictional temperature $T_{iso} = T_g + 61$ °C, we reevaluate a_{iso} with respect to T_{iso} and plot a_{iso} against T_{iso} in Figure 11b. All reevaluated plots coincide reasonably and can be well predicted by the WLF eq 8 (in curve). The WLF parameters are identical for the WLF curves in Figures 10b and 11b.

5. DISCUSSION

5.1. Temperature Dependence of Moduli Contributed from the Decrosslinking. The weaker temperature dependence of the decrosslinking part of modulus compared with the Rouse part of modulus, and accordingly the broadening of plateau region with increasing T, is opposite dramatically to a trend observed earlier for the physical networks based on ionic groups or hydrogen-bondings,[3,54,55] for which the plateau modulus narrows with increasing T. Figure 12a summarizes temperature dependences observed for the precursor, ionomer, and vitrimer. If we ignore a small difference of their T_g, the temperature dependences are essentially the same for the vitrimer, ionomer, and precursor at low T, all reflecting an empirical activation energy for motion of the Rouse segments. In comparison, the temperature dependences are quite different for the decrosslinking parts of modulus of the vitrimer and ionomer at high T; the ionomer and vitrimer exhibit temperature dependences stronger and weaker than that of the precursor, respectively.

The temperature dependence for decrosslinking part of modulus of ionomer was explained by considering the relative change of two time scales, that is, the attempting time τ_0 and the lifetime of network associations τ_s. Because the ionic groups are covalently attached to the backbone of ionomer chains, the ion dissociation is activated by the thermal motion of the polymer segments. As a result, τ_0 and τ_s can be chosen as the Rouse time of Kuhn segment and the lifetime of ionic association, respectively. τ_0 and τ_s are related to the association energy E_a and thermal energy kT as $\tau_s = \tau_0 \exp(E_a/kT)$. Therefore, the decrosslinking part of modulus, governed by τ_s, exhibits temperature dependence stronger than the Rouse part of modulus that is governed by τ_0. The narrowing of plateau

https://dx.doi.org/10.1021/acs.macromol.9b02162
Macromolecules 2020, 53, 1180−1190

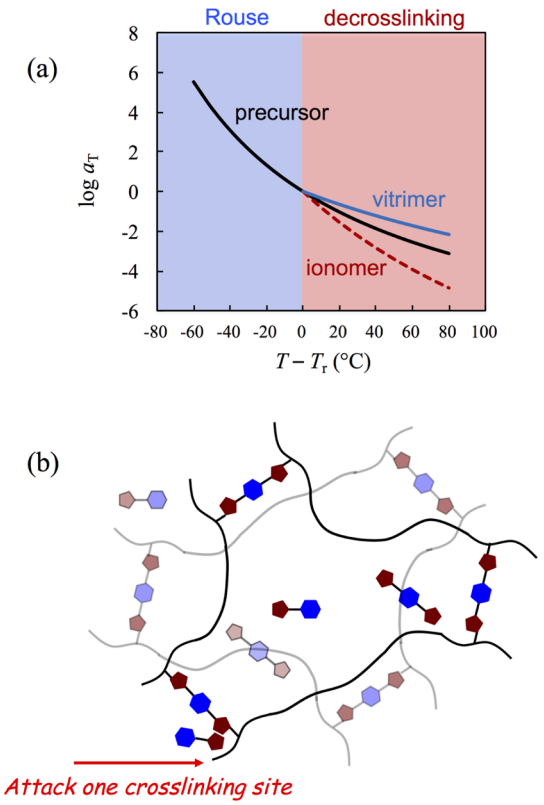

Figure 12. (a) Comparison of the temperature dependences of shift factors a_T of vitrimer, ionomer, and their precursor. The curve shown in the blue region is the shift factor of Rouse part of segment, which is the same for all three systems if we ignore a difference of T_g. The curves shown in the red region are the shift factors of the decrosslinking part of modulus of vitrimer and ionomer, which are different from that of the precursor. (b) Schematic illustration of the decrosslinking reaction where a small molecular byproduct attacks the cross-linking site.

with increasing T simply reflects a reduction of E_a/kT with increasing T.

Following this explanation, we may infer that the activation energy for decrosslinking of vitrimer is lower than that for the segmental motion. This result is counterintuitive considering that the motion of the polymer segments seems to be a prerequisite for the dissociation.

Figure 12b shows schematically the molecular picture of the vitrimer above the gel point in this study. For 1.9−1.4 and 1.9−1.6, whose temperature dependences are utilized for determine E_a, we estimate a ratio of functional groups between cross-linker and precursor $2r/pN$ = 1.5 and 1.7, meaning that functional groups of the cross-linker are in excess with respect to that of the precursor. The redundant cross-linker C and byproduct B can exchange with the cross-linking site. Because the Kuhn segment of PHMA is expected to be ∼8 monomers (evaluated based on the argument that Kuhn segment is about twice the persistent length, and a persistent length has the same number of carbons as the side chain[56]), both the cross-linker and byproduct are much smaller than the Kuhn segment. As a result, the diffusion of either the cross-linker or the byproduct may be associated to an apparent activation energy much lower than that of the Rouse segment of PHMA.

We may regard the decrosslinking reaction as due to effective collision of either the cross-linker or the byproduct with the association sites along specific direction (see, e.g., a collision indicated in arrow in Figure 12b). As the temperature rises, molecular motions speed up for both the polymeric segments and the small molecules. Although the motion of polymeric segments speeds up more, it is still slower than the motion of the small molecules, including the cross-linker and byproduct. Then, the amount of activated small molecules that collide effectively with the cross-linking sites would depend mainly on the increase of their own mobility. As a result, the temperature dependence of the decrosslinking reaction is more associated to the temperature dependence of diffusivity of the small molecules rather than that of the polymeric segments. This feature is different from most of the physical network where the stickers are covalently attached to the polymeric segments, for which the sticker dissociation is strongly correlated to the activation energy for motion of the polymer segments.

Another difference between chemical reaction and physical association is that the former is highly directional; therefore, the chance for the reverse reaction of two broken sites is quite low. In contrast, the interaction between ionic groups is less directional, and thus one broken sticker may reassociate to its original partner several times before finding a new partner.[51] This reassociation has been noted in the recent experimental studies,[3,57] which plays a critical role from a rheological point of view because the stress borne by a strand can be relaxed only if the broken site associates randomly to a new partner. The repeated dissociation−reassociation processes of the ionomer should strengthen the correlation between the characteristic time of decrosslinking and that of segmental motion.

In summary, the broad plateau region indicates that the lifetime of the dynamic covalent bond is significantly larger than the Rouse time of the network strands. Because the reassociation after dissociation is unlikely, the stress relaxation would be realized soon after the dissociation. The dissociation is governed by both the diffusion activation energy of the small molecular cross-linker and byproduct and the activation energy of the dioxaborolane metathesis reaction.

The diffusion of small molecular cross-linker and byproduct in the vitrimer should be slower than that in the small molecular system. In the literature,[49,52] the reaction kinetics was examined on small-molecular model system based on the dioxaborolane metathesis reaction in solution. These experiments confirmed that either water or diol can facilitate the exchange reaction, even when the amount was trivial. It was proposed that hydrolysis of boronic esters generated diols that could catalyze the exchange reaction in situ.[49,52] Analyzing the temperature dependence with Arrhenius equation gave an activation energy of 28.1 kJ/mol.[52] The activation energy had been further reduced through utilizing the less stable 5-membered boronic ester rings instead of 6-membered boronic ester rings as the constructing unit or through introducing nitrogen coordination.[58,59] The activation energy of the polymer systems, determined either by Leibler and co-workers[46] (E_a = 43 ± 4 kJ/mol) or by us (E_a = 52 ± 3 kJ/mol), is larger than those of the small molecular model systems, which possibly reflects the higher activation energy for diffusion of small molecules, such as cross-linker C and byproduct B, in the polymer medium. Following this explanation, we may attribute the slightly higher E_a for 1.9−1.6 than 1.9−1.4 to its higher T_g.

5.2. Relationship between Degree of Gelation and Kinetics of Cross-linking Reaction. Because the degree of

https://dx.doi.org/10.1021/acs.macromol.9b02162
Macromolecules 2020, 53, 1180−1190

gelation can reflect a density of the cross-linking point, we should in turn determine $[P_2C]$ from LVE. To this end, we should first determine a degree of gelation ε. In the Flory–Stockmayer gelation theory, the degree of gelation is defined as $\varepsilon = (p_{eff} - p_c)/p_c$, with the gel point $p_c = 1/(DP - 1) = 1.7\%$ and p_{eff} a number fraction of effectively cross-linked monomers. For 1.9–0.8 and 1.9–6.0 (cf. Figures 6 and 7), LVE is characterized by a broad power-law-type relaxation. In addition, a slight increase of r from 0.8 to 1.2 or decrease of r from 6.0 to 5.3 leads to appearance of a clear plateau region. These features suggest that 1.9–0.8 and 1.9–6.0 are sol samples with p_{eff} very close to p_c. Therefore, we may approximately assign a degree of gelation of $\varepsilon \approx 0$ for r = 0.8 and 6.0.

Above the gel point, there is one important transition occurring at the Ginzburg transition point of $\varepsilon_G = 1/N_{kuhn}^{1/3} = 0.5$, where $N_{kuhn} = M_n/M_{Kuhn}$ is the number of Kuhn segments per precursor chain, with M_n = 10,000 Da and M_{Kuhn} = 1400 Da being MW per chain and per Kuhn segment, respectively. At $\varepsilon_G \le \varepsilon \le 1$, the gel strands are overlapped and the mean-field percolation holds, giving a plateau of $G_N = \varepsilon^3\rho RT/M$ that reduces to $G_0 = \rho RT/M = 10^{5.5}$ Pa at $\varepsilon = 1$ and to $G_G = \rho RT/(MN_{Kuhn}) = 10^{4.6}$ Pa at $\varepsilon = \varepsilon_G = 1/N_{kuhn}^{1/3}$. The difference between G_0 and G_G is small (within one decade), which possibly explains no clear mean-field behavior, $G' \sim G'' \sim \omega$, seen for the two sol samples, that is, 1.9–0.8 and 1.9–6.0. For the 1.9-r vitrimer samples in our study, only 1.9–1.6 and 1.9–3.0 have plateau moduli in between G_G and G_0, indicating that their degree of gelation $\varepsilon_G < \varepsilon < 1$, whereas 1.9–1.2, 1.9–1.4, and 1.9–5.3 have plateau moduli lower than G_G, indicating they have $0 < \varepsilon < \varepsilon_G$.

For 1.9–1.6 and 1.9–3.0 with $\varepsilon_G < \varepsilon < 1$, ε can be calculated inversely from G_N from the scaling law in mean field region[60]

$$\varepsilon = (G_N/G_0)^{1/3} \qquad \text{for } \varepsilon_G \le \varepsilon < 1 \tag{9}$$

For 1.9–1.2, 1.9–1.4, and 1.9–5.3 with $\varepsilon < \varepsilon_G$, ε can be calculated inversely from G_N from the scaling law in critical percolation region[61]

$$\varepsilon = \varepsilon_G(G_N/G_G)^{1/2.7} \qquad \text{for } 0 < \varepsilon < \varepsilon_G \tag{10}$$

ε thus determined (from G_N) are summarized in Table 2. From ε, we can calculate $p_{eff} = (\varepsilon + 1)p_c$ and accordingly the number density of two-site cross-linking $[P_2C] = \nu p_{eff}N/2 = \nu(\varepsilon + 1)p_cN/2 = \nu(\varepsilon + 1)N/[2(N - 1)]$, where ν is the number density of precursor chain and 2 in denominator means that to form each P_2C consumes two polymer sites. Considering that the original polymer sites is $C = pN\nu$, where $pN = 1.9$ is the number of sites per chain, we have $[P_2C]/C = (\varepsilon + 1)/[2p(N - 1)]$.

The same analysis has also been given on LVE of the 3.1-r samples (Figures S7 and S8). Figure 13 plots $[P_2C]/C$ thus-determined against r (in sphere symbol) for both the 1.9-r (panel a) and 3.1-r (panel b) samples. To our surprise, $[P_2C]/C$ thus-determined agrees reasonably with a prediction assuming $K_1 = 1$ and $K_2 = 10$, rather than $K_1 = 1$ and $K_2 = 1$ that have been frequently assumed for the exchange reaction.[44] This result means that to form two-site cross-linking point is preferred than the single-site cross-linking point. Although we are not sure about the mechanism, we know that higher K_2 means that either the forward second-step reaction has been facilitated or the backward second-step reaction has been suppressed. On the one hand, the forward

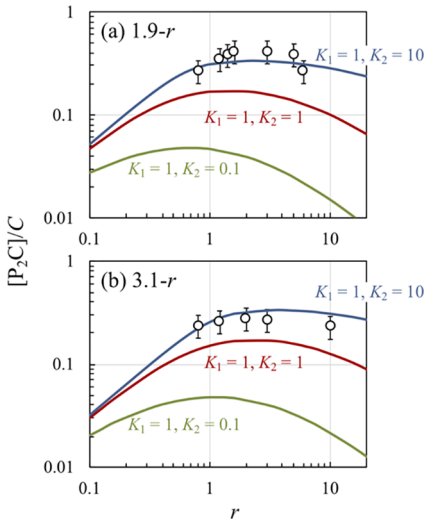

Figure 13. Plots of $[P_2C]/C$ of the (a) 1.9-r and (b) 3.1-r vitrimers against r, where $[P_2C]/C$ calculated from LVE and predicted from theory are shown in symbol and curve, respectively.

reaction might be facilitated by aggregation of the polymer sites, including P, PC, and P_2C sites, to enhance their localized concentrations. In other words, [PC] and [P] could be larger than the average concentration in the system so as to increase a chance for collision between P and PC sites in the second step reaction. We conducted the X-ray scattering measurements to check the aggregation. However, there is no clear sign of the aggregation in the scattering measurements (see Figure S10 of the Supporting Information), but this does not necessarily mean that there is no aggregation because the appearance of aggregation peak in the X-ray scattering also relies on sufficient contrast of electron density between the aggregate and the matrix. On the other hand, it is also possible that the cross-linking P_2C site has much lower mobility than the PC site formed in the first step reaction. This would make the collision more difficult in between the P_2C and B sites, thereby suppressing the backward reaction. In other words, the backward second-step reaction (between P_2C and B) is slower than the backward first-step reaction (between PC and B) to give higher K_2 than K_1.

For the gel sample, the average molecular weight per strand M_s can be evaluated from the plateau modulus G_N as: $P_{gel}\rho RT/M_s = G_N$, where P_{gel} is a fraction of chains that are incorporated into the gel (and $1 - P_{gel}$ is the fraction of chains that are either the sol chains or the solvent). Because $P_{gel} \approx 0$ at the gel point, where the degree of gelation $\varepsilon = 0$, and $P_{gel} \approx 1$ at the full gelation point, where $\varepsilon = 1$, the mean-field theory predicts $P_{gel} = \varepsilon$ and $M_s = \varepsilon\rho RT/G_N$. The values of M_s thus estimated are summarized in Table 2. For all of the gel samples in this study, we found that M_s is larger than M_n of the precursor, meaning that each network strand is composed of several precursor chains on average. Probably, these mutually connected chains would take a branched structure.

6. CONCLUDING REMARKS

In summary, we examined linear viscoelasticity of the vitrimer samples based on the dioxaborolane metathesis reaction. We found that the temperature dependence of the terminal relaxation is weaker than that of the Rouse segment. We presumed that the low temperature dependence of decrosslinking is attributed to the low activation energy for both the

https://dx.doi.org/10.1021/acs.macromol.9b02162
Macromolecules 2020, 53, 1180–1190

dioxaborolane metathesis reaction and the diffusion of small molecules, including the cross-linker and the byproduct that are much smaller than the Kuhn segments of the polymer. These small molecules can exchange with the cross-linking sites to activate the decrosslinking reaction, endowing the vitrimers with superior processability. We also noted that the reaction constant is higher for the second step than the first step reaction. We hypothetically attribute this to the aggregation of the polymer sites and/or the low mobility of the dual-crosslinking points. This study shows that excess of cross-linker molecules can make vitrimers again flowable/processable, which suggests a convenient pathway to reuse/recycle the covalent adaptable network.

■ ASSOCIATED CONTENT

Supporting Information

The Supporting Information is available free of charge at https://pubs.acs.org/doi/10.1021/acs.macromol.9b02162.

Synthesis and characterization of the precursor and cross-linker; linear viscoelasticity of the 0.7-*r* and 3.1-*r* vitrimers; test of tTs of the 1.9−1.6 sample; and X-ray scattering profiles of the vitrimer samples (PDF)

■ AUTHOR INFORMATION

Corresponding Author

Quan Chen − *Chinese Academy of Sciences, Changchun Institute of Applied Chemistry, State Key Lab of Polymer Physics and Chemistry, Changchun Institute of Applied Chemistry, Changchun 130022, Jilin, China;* orcid.org/0000-0002-7771-5050; Email: qchen@ciac.ac.cn

Authors

Shilong Wu − *Chinese Academy of Sciences, Changchun Institute of Applied Chemistry, State Key Lab of Polymer Physics and Chemistry, Changchun Institute of Applied Chemistry, Changchun 130022, Jilin, China*

Huanhuan Yang − *Chinese Academy of Sciences, Changchun Institute of Applied Chemistry, State Key Lab of Polymer Physics and Chemistry, Changchun Institute of Applied Chemistry, Changchun 130022, Jilin, China*

Shaoyong Huang − *Chinese Academy of Sciences, Changchun Institute of Applied Chemistry, State Key Lab of Polymer Physics and Chemistry, Changchun Institute of Applied Chemistry, Changchun 130022, Jilin, China;* orcid.org/0000-0001-8210-8928

Complete contact information is available at: https://pubs.acs.org/10.1021/acs.macromol.9b02162

Notes

The authors declare no competing financial interest.

■ ACKNOWLEDGMENTS

Q.C. acknowledges National Natural Science Foundation of China (21722407) and (21674117). We would like to thank Prof. Tadashi Inoue from Osaka Univ. for the insightful discussion of the equilibrium constants.

■ REFERENCES

(1) Rubinstein, M.; Colby, R. H. *Polymer Physics*; Oxford University Press: New York, 2003.

(2) Israelachvili, J. N. *Intermolecular and Surface Forces*, 3rd ed.; Academic Press: Burlington, MA, 2011.

(3) Zhang, Z.; Liu, C.; Cao, X.; Gao, L.; Chen, Q. Linear Viscoelastic and Dielectric Properties of Strongly Hydrogen-Bonded Polymers near the Sol-Gel Transition. *Macromolecules* **2016**, *49*, 9192−9202.

(4) Lewis, C. L.; Stewart, K.; Anthamatten, M. The Influence of Hydrogen Bonding Side-Groups on Viscoelastic Behavior of Linear and Network Polymers. *Macromolecules* **2014**, *47*, 729−740.

(5) Madhavan, P.; Peinemann, K.-V.; Nunes, S. P. Complexation-Tailored Morphology of Asymmetric Block Copolymer Membranes. *ACS Appl. Mater. Interfaces* **2013**, *5*, 7152−7159.

(6) Osterwinter, C.; Schubert, C.; Tonhauser, C.; Wilms, D.; Frey, H.; Friedrich, C. Rheological Consequences of Hydrogen Bonding: Linear Viscoelastic Response of Linear Polyglycerol and Its Permethylated Analogues as a General Model for Hydroxyl-Functional Polymers. *Macromolecules* **2015**, *48*, 119−130.

(7) Staropoli, M.; Raba, A.; Hövelmann, C. H.; Krutyeva, M.; Allgaier, J.; Appavou, M.-S.; Keiderling, U.; Stadler, F. J.; Pyckhout-Hintzen, W.; Wischnewski, A.; Richter, D. Hydrogen Bonding in a Reversible Comb Polymer Architecture: A Microscopic and Macroscopic Investigation. *Macromolecules* **2016**, *49*, 5692−5703.

(8) Wang, X.; Bazuin, C. G.; Pellerin, C. Effect of small molecule hydrogen-bond crosslinker and solvent power on the electrospinnability of poly(4-vinyl pyridine). *Polymer* **2015**, *57*, 62−69.

(9) Ikkala, O.; Ruokolainen, J.; Torkkeli, M.; Tanner, J.; Serimaa, R.; ten Brinke, G. Ordering in self-organizing comb copolymer-like systems obtained by hydrogen bonding between charged or noncharged polymers and amphiphiles. *Colloids Surf., A* **1999**, *147*, 241−248.

(10) Shabbir, A.; Goldansaz, H.; Hassager, O.; van Ruymbeke, E.; Alvarez, N. J. Effect of Hydrogen Bonding on Linear and Nonlinear Rheology of Entangled Polymer Melts. *Macromolecules* **2015**, *48*, 5988−5996.

(11) Wu, S.; Liu, S.; Zhang, Z.; Chen, Q. Dynamics of Telechelic Ionomers with Distribution of Number of Ionic Stickers at Chain Ends. *Macromolecules* **2019**, *52*, 2265−2276.

(12) Helen, J.-H. Ion States and Transport in Styrenesulfonate Methacrylic PEO9 Random Copolymer Ionomers. *Macromolecules* **2015**, *48*, 7273−7285.

(13) Shabbir, A.; Huang, Q.; Baeza, G. P.; Vlassopoulos, D.; Chen, Q.; Colby, R. H.; Alvarez, N. J.; Hassager, O. Nonlinear shear and uniaxial extensional rheology of polyether-ester-sulfonate copolymer ionomer melts. *J. Rheol.* **2017**, *61*, 1279−1289.

(14) Weiss, R. A.; Zhao, H. Rheological Behavior of Oligomeric Ionomers. *J. Rheol.* **2009**, *53*, 191−213.

(15) Seitz, M. E.; Chan, C. D.; Opper, K. L.; Baughman, T. W.; Wagener, K. B.; Winey, K. I. Nanoscale Morphology in Precisely Sequenced Poly(ethylene-co-acrylic acid) Zinc Ionomers. *J. Am. Chem. Soc.* **2010**, *132*, 8165−8174.

(16) Rao, Y.-L.; Chortos, A.; Pfattner, R.; Lissel, F.; Chiu, Y.-C.; Feig, V.; Xu, J.; Kurosawa, T.; Gu, X.; Wang, C.; He, M.; Chung, J. W.; Bao, Z. Stretchable Self-Healing Polymeric Dielectrics Cross-Linked Through Metal-Ligand Coordination. *J. Am. Chem. Soc.* **2016**, *138*, 6020−6027.

(17) Brassinne, J.; Gohy, J.-F.; Fustin, C.-A. Orthogonal Control of the Dynamics of Supramolecular Gels from Heterotelechelic Associating Polymers. *ACS Macro Lett.* **2016**, *5*, 1364−1368.

(18) Tang, Z.; Huang, J.; Guo, B.; Zhang, L.; Liu, F. Bioinspired Engineering of Sacrificial Metal−Ligand Bonds into Elastomers with Supramechanical Performance and Adaptive Recovery. *Macromolecules* **2016**, *49*, 1781−1789.

(19) Han, K.; Go, D.; Hoenders, D.; Kuehne, A. J. C.; Walther, A. Switchable Supracolloidal Coassembly of Microgels Mediated by Host/Guest Interactions. *ACS Macro Lett.* **2017**, *6*, 310−314.

(20) Zhang, J.; Sun, H.; Ma, P. X. Host-Guest Interaction Mediated Polymeric Assemblies: Multifunctional Nanoparticles for Drug and Gene Delivery. *ACS Nano* **2010**, *4*, 1049−1059.

(21) Kakuta, T.; Takashima, Y.; Sano, T.; Nakamura, T.; Kobayashi, Y.; Yamaguchi, H.; Harada, A. Adhesion between Semihard Polymer

Materials Containing Cyclodextrin and Adamantane Based on Host–Guest Interactions. *Macromolecules* **2015**, *48*, 732–738.
(22) Nakahata, M.; Takashima, Y.; Yamaguchi, H.; Harada, A. Redox-responsive self-healing materials formed from host-guest polymers. *Nat. Commun.* **2011**, *2*, 511.
(23) Chen, X.; Dam, M. A.; Ono, K.; Mal, A.; Shen, H. B.; Nutt, S. R.; Sheran, K.; Wudl, F. A thermally re-mendable cross-linked polymeric material. *Science* **2002**, *295*, 1698–1702.
(24) Chen, X.; Wudl, F.; Mal, A. K.; Shen, H.; Nutt, S. R. New thermally remendable highly cross-linked polymeric materials. *Macromolecules* **2003**, *36*, 1802–1807.
(25) Bowman, C. N.; Kloxin, C. J. Covalent adaptable networks: reversible bond structures incorporated in polymer networks. *Angew. Chem.* **2012**, *51*, 4272–4274.
(26) Kloxin, C. J.; Scott, T. F.; Adzima, B. J.; Bowman, C. N. Covalent Adaptable Networks (CANs): A Unique Paradigm in Crosslinked Polymers. *Macromolecules* **2010**, *43*, 2643–2653.
(27) Martin, R.; Rekondo, A.; Ruiz de Luzuriaga, A.; Cabañero, G.; Cabañero, H. J.; Odriozola, I. The processability of a poly(urea-urethane) elastomer reversibly crosslinked with aromatic disulfide bridges. *J. Mater. Chem. A* **2014**, *2*, 5710–5715.
(28) de Luzuriaga, A. R.; Martin, R.; Markaide, N.; Rekondo, A.; Cabanero, G.; Rodriguez, J.; Odriozola, I. Epoxy resin with exchangeable disulfide crosslinks to obtain reprocessable, repairable and recyclable fiber-reinforced thermoset composites. *Mater. Horiz.* **2016**, *3*, 241–247.
(29) Brutman, J. P.; Delgado, P. A.; Hillmyer, M. A. Polylactide Vitrimers. *ACS Macro Lett.* **2014**, *3*, 607–610.
(30) Chen, Q.; Li, Y.; Yang, Y.; Xu, Y.; Qian, X.; Wei, Y.; Ji, Y. Durable liquid-crystalline vitrimer actuators. *Chem. Sci.* **2019**, *10*, 3025–3030.
(31) Yang, Y.; Pei, Z.; Li, Z.; Wei, Y.; Ji, Y. Making and Remaking Dynamic 3D Structures by Shining Light on Flat Liquid Crystalline Vitrimer Films without a Mold. *J. Am. Chem. Soc.* **2016**, *138*, 2118–2121.
(32) Capelot, M.; Montarnal, D.; Tournilhac, F.; Leibler, L. Metal-catalyzed transesterification for healing and assembling of thermosets. *J. Am. Chem. Soc.* **2012**, *134*, 7664–7667.
(33) Denissen, W.; Rivero, G.; Nicolaÿ, R.; Leibler, L.; Winne, J. M.; Du Prez, F. E. Vinylogous Urethane Vitrimers. *Adv. Funct. Mater.* **2015**, *25*, 2451–2457.
(34) Denissen, W.; Droesbeke, M.; Nicolay, R.; Leibler, L.; Winne, J. M.; Du Prez, F. E. Chemical control of the viscoelastic properties of vinylogous urethane vitrimers. *Nat. Commun.* **2017**, *8*, 14857.
(35) Taynton, P.; Yu, K.; Shoemaker, R. K.; Jin, Y.; Qi, H. J.; Zhang, W. Heat- or water-driven malleability in a highly recyclable covalent network polymer. *Adv. Mater.* **2014**, *26*, 3938–3942.
(36) Zheng, N.; Fang, Z.; Zou, W.; Zhao, Q.; Xie, T. Thermoset Shape-Memory Polyurethane with Intrinsic Plasticity Enabled by Transcarbamoylation. *Angew. Chem., Int. Ed.* **2016**, *55*, 11421–11425.
(37) Fortman, D. J.; Brutman, J. P.; Cramer, C. J.; Hillmyer, M. A.; Dichtel, W. R. Mechanically activated, catalyst-free polyhydroxyurethane vitrimers. *J. Am. Chem. Soc.* **2015**, *137*, 14019–14022.
(38) Yuan, C. E.; Zhang, M. Q.; Rong, M. Z. Application of alkoxyamine in self-healing of epoxy. *J. Mater. Chem. A* **2014**, *2*, 6558–6566.
(39) Wojtecki, R. J.; Meador, M. A.; Rowan, S. J. Using the dynamic bond to access macroscopically responsive structurally dynamic polymers. *Nat. Mater.* **2011**, *10*, 14–27.
(40) Zheng, N.; Hou, J. J.; Zhao, H. B.; Wu, J. J.; Luo, Y. W.; Bai, H.; Rogers, J. A.; Zhao, Q.; Xie, T. Mechano-Plastic Pyrolysis of Dynamic Covalent Polymer Network toward Hierarchical 3D Ceramics. *Adv. Mater.* **2019**, *31*, 1807326.
(41) Cromwell, O. R.; Chung, J.; Guan, Z. Malleable and Self-Healing Covalent Polymer Networks through Tunable Dynamic Boronic Ester Bonds. *J. Am. Chem. Soc.* **2015**, *137*, 6492–6495.
(42) Deng, R.; Derry, M. J.; Mable, C. J.; Ning, Y.; Armes, S. P. Using Dynamic Covalent Chemistry To Drive Morphological Transitions: Controlled Release of Encapsulated Nanoparticles from Block Copolymer Vesicles. *J. Am. Chem. Soc.* **2017**, *139*, 7616–7623.
(43) Ricarte, R. G.; Tournilhac, F.; Leibler, L. Phase Separation and Self-Assembly in Vitrimers: Hierarchical Morphology of Molten and Semicrystalline Polyethylene/Dioxaborolane Maleimide Systems. *Macromolecules* **2019**, *52*, 432–443.
(44) Kloxin, C. J.; Bowman, C. N. Covalent adaptable networks: smart, reconfigurable and responsive network systems. *Chem. Soc. Rev.* **2013**, *42*, 7161–7173.
(45) Montarnal, D.; Capelot, M.; Tournilhac, F.; Leibler, L. Silica-Like Malleable Materials from Permanent Organic Networks. *Science* **2011**, *334*, 965–968.
(46) Röttger, M.; Domenech, T.; van der Weegen, R.; Breuillac, A.; Nicolaÿ, R.; Leibler, L. High-performance vitrimers from commodity thermoplastics through dioxaborolane metathesis. *Science* **2017**, *356*, 62–65.
(47) Bapat, A. P.; Roy, D.; Ray, J. G.; Savin, D. A.; Sumerlin, B. S. Dynamic-covalent macromolecular stars with boronic ester linkages. *J. Am. Chem. Soc.* **2011**, *133*, 19832–19838.
(48) Cash, J. J.; Kubo, T.; Bapat, A. P.; Sumerlin, B. S. Room-Temperature Self-Healing Polymers Based on Dynamic-Covalent Boronic Esters. *Macromolecules* **2015**, *48*, 2098–2106.
(49) Ogden, W. A.; Guan, Z. Recyclable, Strong, and Highly Malleable Thermosets Based on Boroxine Networks. *J. Am. Chem. Soc.* **2018**, *140*, 6217–6220.
(50) Chen, Y.; Tang, Z.; Liu, Y.; Wu, S.; Guo, B. Mechanically Robust, Self-Healable, and Reprocessable Elastomers Enabled by Dynamic Dual Cross-Links. *Macromolecules* **2019**, *52*, 3805–3812.
(51) Stukalin, E. B.; Cai, L.-H.; Kumar, N. A.; Leibler, L.; Rubinstein, M. Self-Healing of Unentangled Polymer Networks with Reversible Bonds. *Macromolecules* **2013**, *46*, 7525–7541.
(52) Roettger, M. Associative Exchange Reactions of Boron or Nitrogen Containing Bonds and Design of Vitrimers. Ph.D. Thesis, Pierre and Marie Curie University, 2018.
(53) Lusignan, C. P.; Mourey, T. H.; Wilson, J. C.; Colby, R. H. Viscoelasticity of Randomly Branched Polymers in the Critical Percolation Class. *Phys. Rev. E: Stat., Nonlinear, Soft Matter Phys.* **1995**, *52*, 6271–6280.
(54) Zhang, Z.; Huang, C.; Weiss, R. A.; Chen, Q. Association Energy in Strongly Associative Polymers. *J. Rheol.* **2017**, *61*, 1199–1207.
(55) Zhang, Z.; Chen, Q.; Colby, R. H. Dynamics of associative polymers. *Soft Matter* **2018**, *14*, 2961–2977.
(56) Rathgeber, S.; Pakula, T.; Wilk, A.; Matyjaszewski, K.; Beers, K. L. On the shape of bottle-brush macromolecules: Systematic variation of architectural parameters. *J. Chem. Phys.* **2005**, *122*, 124904.
(57) Gold, B. J.; Hövelmann, C. H.; Lühmann, N.; Székely, N. K.; Pyckhout-Hintzen, W.; Wischnewski, A.; Richter, D. Importance of Compact Random Walks for the Rheology of Transient Networks. *ACS Macro Lett.* **2017**, *6*, 73–77.
(58) Bao, C.; Jiang, Y.-J.; Zhang, H.-Y.; Lu, X. Y.; Sun, J. Q. Room-Temperature Self-Healing and Recyclable Tough Polymer Composites Using Nitrogen-Coordinated Boroxines. *Adv. Funct. Mater.* **2018**, *28*, 1800560.
(59) Bao, C.; Guo, Z.; Sun, H.; Sun, J. Nitrogen-Coordinated Boroxines Enable the Fabrication of Mechanically Robust Supramolecular Thermosets Capable of Healing and Recycling under Mild Conditions. *ACS Appl. Mater. Interfaces* **2019**, *11*, 9478–9486.
(60) Rubinstein, M.; Semenov, A. N. Thermoreversible Gelation in Solutions of Associating Polymers. 2. Linear Dynamics. *Macromolecules* **1998**, *31*, 1386–1397.
(61) Chen, Q.; Huang, C.; Weiss, R. A.; Colby, R. H. Viscoelasticity of Reversible Gelation for Ionomers. *Macromolecules* **2015**, *48*, 1221–1230.

https://dx.doi.org/10.1021/acs.macromol.9b02162
Macromolecules 2020, 53, 1180–1190